COMMUTATIONAL RAMP LOAD CONTROL USING A CONVENTIONAL DISC DRIVE ACTUATOR [1]

Ryan Ratliff Prabhakar Pagilla

School of Mechanical and Aerospace Engineering
Oklahoma State University, Stillwater, OK, USA
ryan.ratliff@okstate.edu pagilla@ceat.okstate.edu

Abstract: The research investigates the feasibility of a ramp load/unload (L/UL) controller using a conventional, non-L/UL disc drive actuator. Therefore, disc drives with lower cost, higher torque actuators can realize the shock resistance benefits of ramp loading. A disc drive designed with a conventional actuator is outfitted with a ramp and optimized for L/UL operation. While on the ramp, there exists a set in the state space where the actuator dynamics are uncontrollable. Additionally, there exists two equilibrium points which are functions of the input saturation level. State trajectories are generated that, when tracked, move the actuator through the uncontrollable set and equilibrium points for a successful load onto the disc at the desired load velocity. A trajectory generation methodology is proposed to produce the required state reference trajectories. A continuous, state-feedback controller with varying gains is designed for tracking. A unique disc drive is manufactured that contains both a conventional actuator and ramp load capability. Experiments are conducted to verify the design and modeling results.

Keywords: Ramp load, Disk drive, Trajectory generation, Commutation, Head load

1. INTRODUCTION

The read/write heads of a hard disc drive are very sensitive to external shock and vibration. Shock and vibration dynamics can cause head/disc impact (HDI). If the impact occurs in the area where data is stored, data loss or permanent damage can occur. Typically, there is a maximum shock and vibration specification limit that corresponds to a given head design. Shock specifications are given for both operational and non-operational states. Disc drives will usually be subject to higher shock levels during the non-operational state primarily resulting from shipping and handling. During this process, the drive could incur dynamics from both linear and rotational shocks. In order to prevent damage and data loss, disc drive manufacturers have developed methods to handle external, non-operational dynamics. To combat rotational shocks, external locking or latching mechanism are implemented that hold the disc drive actuator and read/write (R/W) heads at the disc inner radius in the absence of power. To provide linear shock robustness, the R/W heads rest on a "textured", circumferential band at the inner diameter of the disc. The texture prevents any adherence of the R/W head to the disc and provides an area of contact away from the data zone in the presence of linear shocks. Therefore, any HDI will occur in the texture zone where no data is present. These methods have proven to be relatively effective and are currently used in enterprise and server-class drives susceptible to less frequent, low amplitude shock levels. However, drives scheduled for notebook computers and consumer electronic devices will naturally experience higher shock levels. Frequent and severe HDI will cause media divots in the zone textured area. When power is applied and the discs begin to spin, these divots can disrupt the airflow and actually contact the heads causing catastrophic failure during the spin-up process. To combat the issue, many disc drive manufacturers prefer to keep the heads completely off the discs when the drive is not operating. The common method adopted in industry is to park the tip of the actuator on a ramp located outside the disc outer diameter (Pejcha 1976).

A typical non-operational configuration exists with actuator parked on a ramp and heads suspended off the discs. When the drive is powered on, the actuator is moved off the ramp and the heads are loaded onto the discs where normal operation occurs. When the drive is powered off, residual energy from the spindle motor back-emf is used to move the actuator, unloading the heads off the discs and onto the ramp. One issue that has had much attention recently is the effects of HDI during the loading process and how to prevent it. It has been shown that HDI during loading is primarily dependent on vertical loading velocity along with the pitch and roll angle of the head (Jeong and Bogy 1992, Zeng and Bogy

[1] This work was supported in part by the U.S. National Science Foundation under Grant No. CMS 9982071. The authors would like to thank Seagate Technology for providing resources to help make this work possible.

2000). These two factors are a function of the head suspension spring constant, actuator angular velocity, and the ramp incline (Levi and Talke 1992). The suspension spring force is a very controlled parameter because of the effects of aerodynamics and fly height during operation. It is not likely that this parameter will be adjusted to compensate for ramp loading. Additionally, the ramp incline can be restricted by the geometric limitations of the drive form factor. There is flexibility, however, on the angular velocity parameter and disc drive L/UL controllers typically regulate the velocity moving on and off the ramp. This is usually accomplished by direct feedback of the motor back-emf into the controller. The shape of the motor back-emf or torque factor across the actuator stroke (sweep angle) is dependent on the geometry of the magnets. Most L/UL disc drives will have relatively constant torque factors within the normal operating stroke on the disc and reduce to a lower value on the ramp. Therefore, it is advantageous to have an idea of the torque factor characteristics across the entire stroke to promote accurate velocity measurements.

Disc drive actuator magnets are polarized such that the gap flux density is equal and opposite for each of the two coil lengths inside the air gap. The location where the magnet polarity changes is called the magnetic transition (MT). Because the magnetic flux flow in the air gap has opposite direction on each side of the MT, current flowing through the coil produces a force in the active lengths. Each active coil length contributes, roughly, one-half of the total torque produced by the actuator. If the actuator continues to rotate, one active length will cross the magnetic transition where both active lengths are subject to magnetic flux flow in the same direction. In this case, the actuator stops resulting from equal and opposite forces imparted to each coil active length. Because both active coil lengths are influenced equally by similar flux density, the actuator cannot be moved from this position by applying current through the coil. This condition renders the system uncontrollable. Increasing the coil and magnet arc length is a solution that is currently used in industry. The arc length increase effectively changes the MT location and prevents coil overlap which compensates for the extra stroke angle that must be traveled to access the ramp past the outer disc diameter. However, increasing the coil size increases the inertia of the actuator, negatively impacting seek performance. Seek performance is also influenced by magnet surface area. The magnetic air gap flux density is inversely proportional to the magnet surface area. Increasing the magnet surface area effectively reduces the amount of torque generated by the actuator. Also since magnet cost is directly related to the physical volume of material, a cost increase will result from increasing the magnet size. In fact, depending on product sales volume, the cost increase for a given product could be in the millions of dollars. Therefore, implementing the ramp L/UL solution results in a torque reduction along with an inertia increase which are both detrimental to move time performance. Additionally, a significant cost increase is realized from increasing magnet volume. One concept that has been proposed uses a conventional actuator to perform the L/UL operation (Ratliff 2000). It was proposed that current be applied through the coil to move the actuator in a specific direction. Current is then removed from the coil while traveling through the vicinity of the magnetic transition and reapplied with opposite polarity to keep the actuator moving in the same direction. The maneuver is performed open-loop using a series of voltage pulses. The pulse widths and amplitudes are tuned until a successful loading is achieved. However, because of the open-loop nature of the system, there is no knowledge of the actual loading velocity. Furthermore, it may be difficult if not impossible to achieve a desired loading velocity using open-loop voltage pulses. Factors such as disc windage, temperature, and ramp wear could cause large variations in loading velocity over the life of a product.

This research will focus on the development of a closed-loop solution for ramp loading using a conventional disc drive actuator. Therefore, the shock resistance benefits of ramp loading can be realized using lower cost, higher performance actuators. The control problem is particularly challenging because the state space contains an uncontrollable region that must be reached. A reference model of the system is derived and a trajectory generation strategy is developed. The trajectories are designed such that, when tracked, the actuator travels through the uncontrollable condition and successfully loads at the desired velocity. A stable, state-feedback controller is designed to track the trajectories. A unique disc drive was fabricated with a conventional actuator to support ramp loading. Experiments were performed to verify the concept.

2. MODELING

The disc drive actuator under study can be described by a combination of mechanical and electrical dynamic equations. The mechanical dynamics are represented by

$$J\ddot{\theta} = K_m(\theta)i - T_b(\theta) - T_f \ \mathrm{sgn}(\dot{\theta}) \qquad (1)$$

where J is the actuator inertia, and i is the current applied in the coil. The torque factor, K_m, which is relatively constant during operation in the data zone, becomes a function of the actuator arm angle while on the ramp. For the disc drive depicted in Figure 1 there exists a condition rendering the actuator uncontrollable by induced current while traveling on the ramp as discussed in Section 1. The uncontrollable condition occurs at a critical angle, θ_c, corresponding to $K_m(\theta_c) = 0$. The critical angle is measured as the actuator rotates counter-clockwise from the parked position at the outer crash stop (OCS) (Fig 1). Also shown in Figure 1 is a feature that induces a magnetic bias torque on the actuator arm. The bias torque, $T_b(\theta)$, is a function of angle and is required to prevent

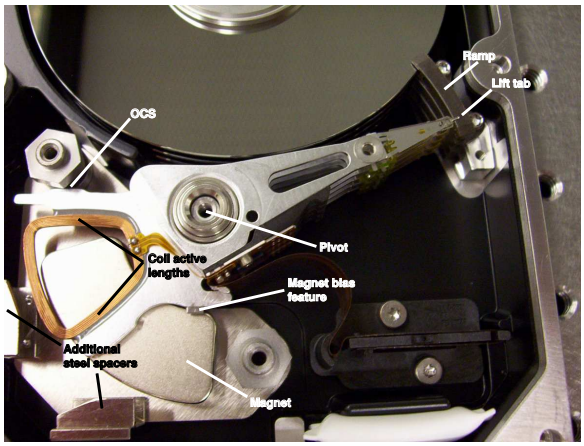

Fig. 1. Conventional disc drive outfitted with ramp. Top magnet removed for clarity

an unrecoverable condition that may be imparted by an external disturbance. The bias assists the actuator in returning to the OCS without requiring current to be present in the coil. The dynamic friction torque, T_f, is present as the suspension lift tab slides across the ramp during a L/UL operation and is dependent on the direction of actuator motion. Equation (2) represents the electrical dynamics where R and L are the coil resistance and inductance, respectively. The supply voltage, V_s, is available for controlling the system.

$$V_s = Ri + L\frac{di}{dt} + K_m(\theta)\dot{\theta} \tag{2}$$

Choosing the states as $x_1 = \theta$, $x_2 = \dot{\theta}$, and $x_3 = i$ gives the third-order state space representation

$$\begin{aligned} \dot{x}_1 &= x_2 \\ \dot{x}_2 &= \tfrac{1}{J}[K_m(x_1)x_3 - T_b(x_1) - T_f \operatorname{sgn}(x_2)] \\ \dot{x}_3 &= \tfrac{1}{L}[-K_m(x_1)x_2 - Rx_3 + u] \end{aligned} \tag{3}$$

There also exists two equilibrium points, x_{1eq-} and x_{1eq+}, depending on the location of the actuator arm relative to the critical angle, θ_c. Equating the left hand side of (3) to zero, shows the equilibrium points occur when

$$K_m(x_{1eq})u_{sat} - RT_b(x_{1eq}) = 0 \tag{4}$$

where u_{sat} is the saturation voltage for the system. By choosing analytical expressions for $K_m(x_1)$ and $T_b(x_1)$, the equilibrium points can be determined as a function of u_{sat} and the coil resistance where $x_{1eq-} < \theta_c < x_{1eq+}$.

3. TRAJECTORY GENERATION

Theoretically, the actuator is uncontrollable at the critical angle, θ_c. An implementation consideration is that there is actually a neighborhood around θ_c where $K_m(\theta)$ is very small and $u \rightarrow u_{sat}$ during tracking. An angle or zone exists, $\Delta\theta_c$, within which the velocity and position states cannot be tracked directly. Therefore, full state tracking control in the traditional sense is not feasible. A trajectory generation strategy must be developed for successful passage of the actuator through $\Delta\theta_c$ while providing smooth, continuous state trajectory functions. For notational clarity, define $\omega = \dot{\theta}$ and $\alpha = \ddot{\theta}$ for the angular velocity and acceleration, respectively. A strategy is proposed that considers the primary constraints of maximum angular loading velocity, ω_l, maximum angular acceleration, α_{max}, and the saturation voltage u_{sat}. The maximum angular acceleration, α_{max}, corresponds to the maximum linear acceleration the read/write head can withstand without damage. It is assumed that $K_m(\theta)$ and $T_b(\theta)$ are known. The total angle the actuator arm travels while on the ramp or ramp loading angle is denoted as θ_r. The loading velocity, ω_l should be achieved prior to the ramp loading angle, θ_r, but subsequent to θ_c. The angle, $\Delta\theta_c$, is chosen as a design parameter and selected so that θ_c is centered within $\Delta\theta_c$. The strategy requires the trajectories be mapped into three sectors based on angular position

$$\mathbb{S}_1 := [0, \theta_-]\,;\ \mathbb{S}_2 := [\theta_-, \theta_+]\,;\ \mathbb{S}_3 := [\theta_+, \theta_r] \tag{5}$$

where $\theta_- = \theta_c - \Delta\theta_c/2$ and $\theta_+ = \theta_c + \Delta\theta_c/2$. Ideally, ω_l, would be achieved as the actuator exits $\mathbb{S}_2$ to minimize the error when the actuator departs the ramp for loading on the disc. It follows that velocity is constant in $\mathbb{S}_3$ ($\omega_{\mathbb{S}3} = \omega_l$) and position is required to vary linearly according to constant velocity. The current trajectory in $\mathbb{S}_3$ is calculated to sustain $\omega_{\mathbb{S}3}$ based on the acceleration required to overcome the bias and frictional torques

$$i_{\mathbb{S}3} = [T_f + T_b(\theta_{\mathbb{S}3}]/K_m(\theta_{\mathbb{S}3}) \tag{6}$$

Since it is known that little or no control effort will be available within $\Delta\theta_c$ ($\mathbb{S}_2$), there is a required initial angular velocity, $\omega_{\mathbb{S}2o}$, upon entering $\mathbb{S}_2$ assuming a linear velocity decay to w_l resulting from magnetic bias and dynamic friction torques. This required angular velocity can be estimated as

$$\omega_{\mathbb{S}2o} = \sqrt{\omega_l^2 + 2(T_{b\theta_c} + T_f)\Delta\theta_c/J} \tag{7}$$

where $T_{b\theta_c}$ is the average bias torque within $\mathbb{S}_2$. While inside $\mathbb{S}_2$, linear velocity decay is observed beginning at $\omega_{\mathbb{S}2o}$ and ending at $\omega_{\mathbb{S}2f} = \omega_l$. The initial and final position $\theta_{\mathbb{S}2o}$ and $\theta_{\mathbb{S}2f}$, respectively, correspond to the boundaries of $\mathbb{S}_2$ and the position trajectory within $\mathbb{S}_2$ is parabolic following from the linear velocity decay. Since current has little effect on the actuator dynamics within $\mathbb{S}_2$, it is advantageous to increase the current to an initial value, $i_{\mathbb{S}3o}$, that will sustain the actuator at ω_l upon entering $\mathbb{S}_3$. Therefore, a smooth trajectory is generated from $i_{\mathbb{S}2o} = 0$ to $i_{\mathbb{S}2f} = i_{\mathbb{S}3o}$. Prior to entering $\mathbb{S}_2$, a smooth trajectory can be generated in $\mathbb{S}_1$ using methods such as those described in (Spong and Vidyasagar 1989) with initial and final conditions $\theta_{\mathbb{S}1o} = \omega_{\mathbb{S}1o} = \alpha_{\mathbb{S}1o} = 0$, $\theta_{\mathbb{S}1f} = \theta_-$, $\omega_{\mathbb{S}1f} = \omega_{\mathbb{S}2o}$, and $\alpha_{\mathbb{S}1f} = (T_f + T_{b\theta_c})/J$. The current is computed from the angular acceleration trajectory as

$$i_{\mathbb{S}1} = J(\alpha_{\mathbb{S}1} - \alpha_{\mathbb{S}1f})/K_m(\theta_{\mathbb{S}1}) \tag{8}$$

Subtraction of $\alpha_{\mathbb{S}1f}$ results in an initial value, $i_{\mathbb{S}1i}$, to immediately compensate for effects of bias and friction. Also, $i_{\mathbb{S}1f} = i_{\mathbb{S}2o} = 0$ to ensure saturation is not reached for small values of $K_m(\theta)$ upon entering

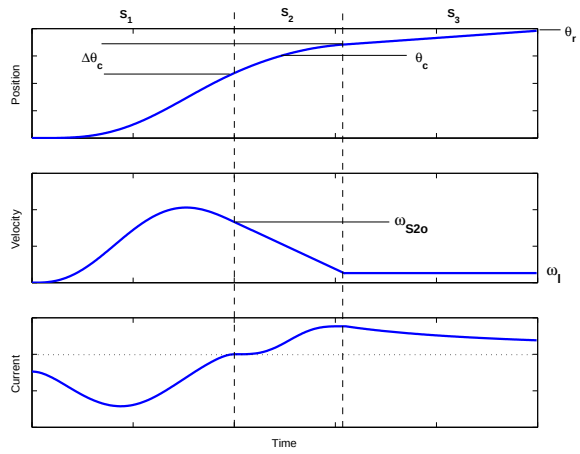

Fig. 2. Example trajectory profiles

$\mathbb{S}_2$. An example trajectory is shown in Figure 2. A summary of the trajectory generation procedure along with additional details about this research project can be found at http://dscl.okstate.edu

4. CONTROLLER DESIGN

A method is required to track the trajectories developed in Section 3 and two controllers are proposed. One controller provides simplicity and acceptable tracking performance while adhering to the constraints outlined in Section 3. The controller is particularly advantageous for systems that are sample rate limited under low disturbance conditions. Another controller provides stability and compensation for small errors that may exist in association with relative differences in torque factor and bias based on reference and actual postion.

The system becomes uncontrollable at θ_c as discussed in Section 2. Additionally, the controller must not exceed u_{sat} which can be problematic when $K_m(\theta)$ becomes small. Using the sector mapping introduced in the previous section, the controller gains can be chosen constant in each sector with smooth, continuous transitions near the sector boundaries. Each sector has individual tracking priorities and the gains can be weighted based on the tracking priority of each state within a sector. For example, it is important to keep the velocity and position error low in $\mathbb{S}_1$. The current tracking performance, however, can be relaxed while only constraining $u < u_{sat}$. Therefore, more weighting can be applied to position and velocity error in $\mathbb{S}_1$. In $\mathbb{S}_2$, because of the controllability condition, the position and velocity trajectories designed in Section 3 assume dynamics from induced current are negligible. An obvious choice for the velocity and position gains would be zero. It is important, however, for current to be driven from $i_{\mathbb{S}2o} = 0$ to $i_{\mathbb{S}2f}$ accurately so that errors are small upon entry into $\mathbb{S}_3$. Weighting on current tracking could be increased in $\mathbb{S}_2$. The resulting control gains take the form $K_j = \{K_j^{\mathbb{S}1} | x_1 \in \mathbb{S}_1\}$, $K_j = \{K_j^{\mathbb{S}2} | x_1 \in \mathbb{S}_2\}$, or $K_j = \{K_j^{\mathbb{S}3} | x_1 \in \mathbb{S}_3\}$ where $K_j^{\mathbb{S}j}$ $(j = 1, 2, 3)$ is constant with smooth, continuous transitions between each sector. Observation of (3) reveals that a sign change in $K_m(x_1)$ requires a sign change in x_3 to maintain consistency with the position and velocity trajectories. Compensation for this requirement is inherent in the current trajectory. However, this is not reflected in the position and velocity trajectories. Therefore, direct multiplication of the position and velocity portion of the control law by $K_m(\theta)$ is necessary to satisfy the requirement. The final control law takes the form

$$u_s = u_{fb} + V_r \tag{9}$$

where $u_{fb} = -K_m(x_1)[K_1(x_1)e_1 + K_2(x_1)e_2] - K_3(x_1)e_3$, $K_1(x_1)$, $K_2(x_1)$, and $K_3(x_1)$ are continuous gain functions, $e_j = x_j - x_{jd}$ is the state tracking error, and x_{jd} is the desired trajectory of the j-th state. The feed-forward reference voltage is represented by

$$V_r = L\dot{x}_{3d} + Rx_{3d} + K_m(x_{1d})x_{2d} \tag{10}$$

Since the torque factor and bias terms in the reference trajectories are based on desired position rather than actual position, additional analysis is required for stability. The following control law

$$u_{sp} = L[K_{1p}(x_1)e_1 + K_{2p}(x_1)e_2 - K_{3p}(x_1)e_3 + \Delta u] + V_r \tag{11}$$

where $K_{jp}(x_1)$ are smooth, continuous gain functions provides stability in $\mathbb{S}_1$ and $\mathbb{S}_3$ when large parameter perturbations are present resulting from position error. An auxiliary control, Δu, is used to compensate for the perturbations. Similar to (9), position and velocity cannot be tracked in $\mathbb{S}_2$ and the gain functions require a transition. The controller derivation with proof is given in the Appendix. Since the addition of Δu adds an extra element of complexity to the controller, the performance benefits may not be justified. For sample rate limited systems not subject to large disturbances, the difference may be small enough to be neglected. Comparison experimental results for both scenarios are presented in the next section.

5. EXPERIMENTS

The trajectories developed in Section 3 and the control law assumes accurate knowledge of the actuator physical parameters. Therefore, measurements were taken of all relevant parameters. Experiments were conducted to verify the performance of the trajectory generation strategy and the proposed controllers.

A ramp was designed and installed in a disc drive with a conventional voice-coil motor actuator that had been optimized for move-time performance within the data stroke angle (Fig. 1). The magnetic circuit assembly was uniquely fabricated in that it allowed for the actuator coil active length to rotate over the magnetic transition. Additional steel spacers were installed behind the coil to provide structural stability for the top magnet assembly while also providing an extra path for magnetic flux, thus improving efficiency of the magnetic circuit. The disc spindle speed was 10,000 rpm. Values for inertia, coil resistance, and coil

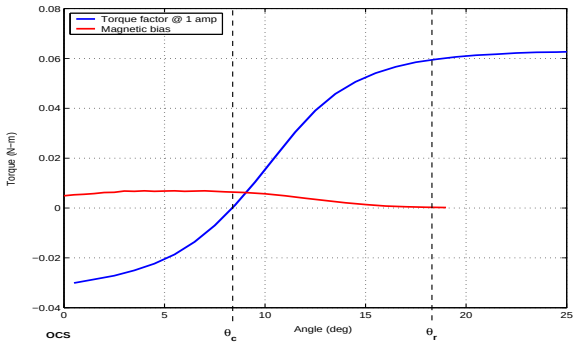

Fig. 3. Torque factor and bias

inductance, were measured at 28.6 g-cm^2, 7.4 Ω, and 0.32 mH, respectively. The lift tab force on the ramp, F_s, was measured at 2.5 grams. A measurement of torque as the lift tab slides across the ramp resulted in a dynamic friction coefficient, $\mu_d = 0.15$. The torque resulting from dynamic friction is $T_f = n\, r_p \mu_d F_s$, where r_p =0.048 m is the distance from actuator pivot to lift tab and $n = 4$ is the number of heads with which the actuator is populated. Beginning with the actuator arm parked at the OCS, the torque factor was measured across the entire stroke angle of approximately 45°. The first 18° of rotation ($\theta_r = 18°$) occurs on the ramp in which the motor torque factor undergoes a sign change. The critical angle was measured at $\theta_c = 8.3°$, where $K_m(\theta_c) = 0$. As discussed previously, the actuator cannot be controlled by current induced in the coil at the critical angle. Therefore, a magnetic bias was designed and optimized on the actuator so that maximum bias torque occurs at θ_c, pulling the actuator back to the OCS, and preventing an unrecoverable situation. Also, it is desired that the bias effects dissipate prior to loading to prevent influence on seek performance ($T_b(\theta) \approx \{0 : \theta > \theta_r\}$). The torque factor and magnetic bias measured along the first 25° of rotation are shown in Figure 3. It becomes apparent from the figure that the static equilibrium points are located where the coil saturation voltage, $u_{sat} = 11$ V, effectively offsets the bias torque.

Computation of the control law was fulfilled by a digital signal processor (DSP) board with analog I/O peripherals. The control voltage was output from the DSP board through a bipolar amplifier and into the ramp L/UL disc drive described previously. Current feedback was achieved by measuring the voltage drop across a 0.2 Ω sense resistor connected in series with the actuator coil. The voltage drop was fed back into the DSP board to calculate the states necessary to update the control law. The velocity was computed based on a measurement of current

$$x_2 = (u - Rx_3)/K_m(x_1) \qquad (12)$$

and integrated to get the position, x_1. The velocity obtained by using (12) was shown to be accurate when compared to laser doppler vibrometer (LDV) measurements and provides a simple, implementable solution. It is evident from (12), however, that the velocity computation can become distorted near θ_c

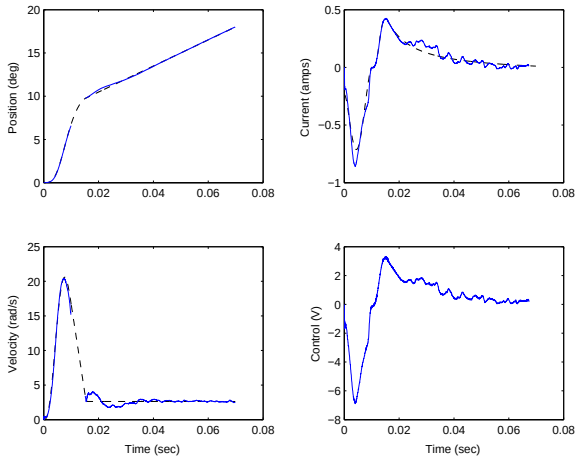

Fig. 4. Results from state-feedback control

when K_m is small. Depending on the noise level of the signals, this becomes another consideration for selecting $\Delta\theta_c$. The sample rate was set at 25 kHz and $\Delta\theta_c$ was chosen to be 3°. The head loading velocity limit was set at 127 mm/s which results in $\omega_l \leq 2.8$ rad/s. The head acceleration limit was 980 m/s^2 corresponding to $\alpha_{max} = 20.4$ krad/s^2. Trajectories were generated based on the procedure discussed in Section 3. The selected control gains are given as $K_1 = \{25000, 0, 5000\}$, $K_2 = \{40, 0, 30\}$, $K_3 = \{0.01, 20, 0.01\}$ for $K_j = \{K_j^{\mathbb{S}1}, K_j^{\mathbb{S}2}, K_j^{\mathbb{S}3}\}$, respectively. A sample of the trajectory tracking performance for a ramp loading maneuver is shown in Figure 4. The figure shows the loading velocity and voltage saturation requirements to be satisfied. Additionally, the maximum angular acceleration imparted to the head was calculated to be $\alpha = 4.67$ krad/s^2 $< \alpha_{max}$. Therefore, all the constraints were satisfied using the state-feedback controller. Because K_m is small in $\mathbb{S}_2$, and K_1 and K_2 are zero, velocity and position were not computed directly in $\mathbb{S}_2$. The region around the ramp cannot be shrouded to direct air flow. Therefore, disc windage can have a significant effect on low velocity tracking in $\mathbb{S}_3$. This is seen as non-periodic "ripple" in the control signal of Figure 4. The ramps used were unfinished, injection mold prototypes which can also have an effect on the controller during low velocity tracking. The error norms using controller (9) are given in Table 1. The norms reflect the weighting strategy discussed in Section 4 where current tracking performance only becomes significant while maneuvering over the uncontrollable region. The controller of (11) was implemented for comparison. Error norm results are shown in Table 1. Control law (11) exhibited slightly improved performance tracking position and velocity. The increase in current error results from the added terms in Δu that compensate for errors in the torque factor and bias relative to the actual and reference trajectories.

6. CONCLUSIONS

The research focused on the design and development of a methodology to provide ramp L/UL functionality

Table 1. Controller performance

L_2 norm	$\mathbb{S}_1$		$\mathbb{S}_2$		$\mathbb{S}_3$	
	u_s	u_{sp}	u_s	u_{sp}	u_s	u_{sp}
e_1	0.02	0.016	-	-	0.06	0.04
e_2	9.33	8.21	-	-	15.57	13.33
e_3	1.42	1.61	0.01	0.01	1.23	1.55

using a conventional disc drive actuator. Implementation of the actuator provides a lower cost, higher torque actuator while realizing the shock resistance benefits of ramp loading. When used in a ramp loading scheme, the conventional actuator exhibits a region that is not controllable by induced coil current. A model reference trajectory generation scheme is developed that, when tracked, moves the actuator through the uncontrollable region for a successful load onto the disc. Two controllers were developed to track the trajectories in the controllable region. A unique disc drive was fabricated to provide ramp loading capability using a conventional actuator. Specific performance specifications were determined for the particular drive under study. Experimental results show that both controllers tracked the trajectories and successfully loaded the R/W heads on the disc while fulfilling the requirement of all constraints. One controller provided a simple, low cost solution where hardware constraints such as sample rate and memory restrictions may be required. Another controller gives a stable solution that compensates for small errors that may occur in real-time calculation of certain physical parameters. In certain instances sufficient trajectories may not be achievable within the given constraints. In such a case the ramp or magnetic bias design will need to be revisited. Although the performance specification were met, it was noted that disc windage had an impact on the controller while tracking at low velocity. Future work will determine other potential trajectory generation schemes that may improve robustness to issues such as disc windage and ramp wear. Also, rather than direct computation, the performance of an observer for estimating the velocity and position states will be investigated. Other controllers will be evaluated to further investigate robustness issues when dealing with population distributions of the actuator physical parameters rather than exact measurements.

Appendix A

The following analysis shows stability for the controller of (11). The dynamics for the ramp load actuator are given by (3). With knowledge of K_m, T_b, and T_f, the reference trajectory dynamics are chosen as

$$\begin{aligned}\dot{x}_{1d} &= x_{2d}\\ \dot{x}_{2d} &= \tfrac{1}{J}[K_m(x_{1d})x_{3d} - T_b(x_{1d}) - T_f\,\mathrm{sgn}(x_{2d})] \quad \text{(A.1)}\\ \dot{x}_{3d} &= \tfrac{1}{L}[-K_m(x_{1d})x_{2d} - Rx_{3d}]\end{aligned}$$

Let $e_j = x_j - x_{jd}$ be the tracking error of the j-th state. Subtracting (A.1) from (3) and substituting $u_{sp} = V_r + Lu_{fb}$ for u gives the error dynamics

$$\begin{aligned}\dot{e}_1 &= e_2\\ \dot{e}_2 &= \tfrac{1}{J}[K_m(x_1)e_3 + \Delta K_m x_{3d} - \Delta T_b - \Delta T_f] \quad \text{(A.2)}\\ \dot{e}_3 &= \tfrac{1}{L}[-K_m(x_1)e_2 - Re_3 - \Delta K_m x_{2d}] + u_{fb}\end{aligned}$$

where $\Delta K_m = K_m(x_1) - K_m(x_{1d})$, $\Delta T_b = T_b(x_1) - T_b(x_{1d})$, $\Delta T_f = T_f\,\mathrm{sgn}(x_2) - T_f\,\mathrm{sgn}(x_{2d})$ and

$$u_{fb} = K_{1p}(x_1)e_1 + K_{2p}(x_1)e_2 - K_{3p}(x_1)e_3 + \Delta u \quad \text{(A.3)}$$

The control law (11) with $K_{1p}(x_1) = J/K_m(x_1)[\gamma_1^2\lambda - \gamma_1^2\gamma_2\lambda]$, $K_{2p}(x_1) = K_m(x_1)/L + J/K_m(x_1)[\gamma_1^2 - \gamma_1\gamma_2\lambda - \gamma_1^2\gamma_2]$, $K_{3p}(x_1) = R/L - \dot{K}_m(x_1)/K_m(x_1) - \lambda - \gamma_1\gamma_2$, and

$$\begin{aligned}\Delta u = \frac{\Delta K_m}{L}x_{2d} - \frac{1}{K_m(x_1)}[&(\Delta K_m)' x_{3d} + \Delta K_m \dot{x}_{3d}\\ &- (\Delta T_b)' + (\lambda + \gamma_1\gamma_2)(\Delta K_m x_{3d} - \Delta T_b - \Delta T_f)]\end{aligned}$$

where $\lambda, \gamma_1 > 0$, $\gamma_2 > 1$ and $(\cdot)'$ denotes $\frac{d(\cdot)}{dt}$ renders the error dynamics (A.2) asymptotically stable in the sectors $\mathbb{S}_1$ and $\mathbb{S}_3$ described in Section 3. Consider the following change of variables:

$$\begin{aligned}s_1 &= e_2 + \lambda e_1\\ s_2 &= \frac{K_m(x_1)}{J}e_3 + \frac{\Delta M}{J} + \lambda e_2 + \gamma_1 s_1 \quad \text{(A.4)}\end{aligned}$$

where $\Delta M = \Delta K_m x_{3d} - \Delta T_b - \Delta T_f$. Differentiating and substituting the error dynamics (A.2) with control law (11), and simplifying gives

$$\begin{bmatrix}\dot{s}_1\\ \dot{s}_2\end{bmatrix} = \begin{bmatrix}-\gamma_1 & 1\\ 0 & (1-\gamma_2)\gamma_1\end{bmatrix}\begin{bmatrix}s_1\\ s_2\end{bmatrix} \quad \text{(A.5)}$$

Therefore, $s_1 \to 0$ and $s_2 \to 0$. Since $s_1 = e_2 + \lambda e_1$ and $\lambda > 0$, $e_1 \to 0$ and $e_2 \to 0$. Notice that e_3 does not converge to zero. From (A.4)

$$e_3 \to -(\Delta K_m x_{3d} - \Delta T_b - \Delta T_f)/K_m(x_1) \quad \text{(A.6)}$$

The variable, s_2, is selected so that the current is used to compensate for any errors that exist in the torque factor and bias relative to the actual and reference position.

REFERENCES

Jeong, T. G. and D. B. Bogy (1992). An experimental study of the parameters that determine slider-disk contacts during dynamic load-unload. *ASME Journal of Tribology* **114**, 507–514.

Levi, P. G. and F. E. Talke (1992). Load/unload investigations on a rotary actuator disk drive. *IEEE Transactions on Magnetics* **28**, 2877–2879.

Pejcha, I. (1976). Head loading and unloading assembly for a magnetic disc drive having a rotary acuator. U.S. Patent 3984873.

Ratliff, R. T. (2000). Extending actuator range through magnetic flux reversal detection. U.S. Patent 6157509.

Spong, M. W. and M. Vidyasagar (1989). *Robot Dynamics and Control*. John Wiley and Sons. New York.

Zeng, Q. H. and D. B. Bogy (2000). Effects of certain design parameters on load/unload performance. *IEEE Transactions on Magnetics* **36**, 140–147.